Anisotropic interference of degenerate four-wave mixing in crystalline silicon

R. Buhleier
Max-Planck-Institut für Festkörperforschung, Heisenbergstrasse 1, 70506 Stuttgart, Germany

G. Lüpke
Institut für Halbleitertechnik, Rheinisch-Westfälische Technische Hochschule Aachen, 52074 Aachen, Germany

G. Marowsky
Laser-Laboratorium Göttingen e.V., Hans-Adolf-Krebs-Weg 1, 37077 Göttingen, Germany

Z. Gogolak
Department of Optics and Quantum Electronics, JATE University, Szeged, Hungary

J. Kuhl
Max-Planck-Institut für Festkörperforschung, Heisenbergstrasse 1, 70506 Stuttgart, Germany
(Received 18 February 1994)

Degenerate-four-wave-mixing experiments have been performed on crystalline silicon at 620 nm using 100-fs pulses. Symmetry analysis has been applied to monitor the fourfold (bulk) symmetry of the [100] direction. Deviations from orthogonal polarization of the pump-and-probe beam with respect to the diffracted-signal beam have been studied in detail. The rotation patterns exhibit the transformation behavior of the relevant $\chi^{(3)}$ tensor. Preliminary time-resolved measurements reveal distinct variations of the signal occurring on a time scale of 10 fs upon excitation with 100-fs pulses, which cannot be detected by standard correlation techniques.

I. INTRODUCTION

Degenerate-four-wave mixing (DFWM) is a widely used experimental technique for investigating both the relative magnitude and the dynamics of nonlinear-optical properties of semiconductors.[1-3] Laser-induced dynamic gratings in silicon have been studied extensively to understand and optimize wave-mixing applications and also to determine material properties such as carrier decay and diffusion times.[4,5] Using different polarizations of the two excitation beams it is possible to generate orientational gratings in which the excited states are predominantly of one orientation in any given local region of the sample, while the direction of the preferred orientation is modulated inside the sample.[6] It has been demonstrated experimentally that the use of polarization properties opens new possibilities for the picosecond and femtosecond time-resolved spectroscopy in semiconductors.[7,8]

DFWM is described by a third-order nonlinear polarization, which is nonzero in the bulk of centrosymmetric materials, like crystalline silicon, and in contrast to the (isotropic) linear polarization it displays anisotropic behavior. The third-order susceptibility $\vec{\chi}^{(3)}$ of cubic semiconductors is perhaps more interesting than $\vec{\chi}^{(2)}$ since there are two nonzero independent elements of $\vec{\chi}^{(3)}$ (for DFWM) given by $\chi^{(3)}_{1111} \equiv A$ and $3\chi^{(3)}_{1212} \equiv B$, and from which we can define the anisotropic parameter $\sigma \equiv (B-A)/A$ that vanishes for an isotropic system.[9] Since the anisotropy is a relative quantity, it is easier to determine experimentally than the absolute magnitude of $\vec{\chi}^{(3)}$, and it is interesting because it is not determined by symmetry, but rather is sensitive to the microscopic electronic properties of the solid. These characteristics have contributed to the recent interest in using optical third-harmonic generation (THG) as a microscopic probe of crystal structure and symmetry in ion-implanted and amorphous silicon.[10-12] To date, however, the only measurements of the anisotropy in $\vec{\chi}^{(3)}$ for silicon have been performed either at $\lambda \approx 10.6\ \mu$m using difference frequency mixing[13-15] or for wavelengths $0.72 < \lambda < 1.92\ \mu$m using THG.[10,16,17] To examine σ for silicon at shorter wavelength ($\lambda = 0.62\ \mu$m), we have become interested in using DFWM, which allows observation of a diffracted signal in transmission from a 10-μm-thick silicon crystal.

Our experimental results refer to a two-beam self-diffraction geometry with 100-fs optical pulses that allows both temporal studies by delaying one pump-beam pulse against its counterpart or changing the polarization configuration of the interacting beams. Hence, the forward DFWM geometry was applied in all experiments at a small intersection angle of 3° in order to achieve near phase matching and to reduce the amount of scattered light.

This paper will be organized as follows: after a short introduction into the theory of the relevant $\vec{\chi}^{(3)}$ symmetry properties with respect to the [100] direction, we present experimental results as to the structural and polarization dependence of the observed DFWM signal under femtosecond excitation. The obvious similarities between changes in the polarization conditions and variation of the delay between the pump-and-probe pulses will

then be discussed. These time-resolved measurements indicate that symmetry analysis is capable of detecting relaxation phenomena much faster than the laser pulse duration t_p in the presence of two competing relaxation channels with relaxation times $\tau_2 \neq \tau_1$ with $\tau_1, \tau_2 \leq t_p$. In our particular experiment, we could resolve momentum randomization of free electrons and holes in Si occurring on a time scale of 10 fs upon excitation with 100-fs pulses and could differentiate between momentum randomization and intraband energy relaxation.

II. EXPERIMENTAL METHODS

The experiments were performed using a standard colliding-pulse mode-locked dye laser (CPM) (Ref. 18) with an intracavity four-prism sequence[19] to provide dispersion compensation. The CPM produced such pulses with a bandwidth-limited duration of $\tau_p \approx 70$ fs at $\lambda \approx 620$ nm, an average power of 30 mW per beam and at a repetition rate of 120 MHz. These pulses were amplified in a conventional six-pass "bow-tie" dye amplifier[20] pumped by a copper vapor laser at a repetition rate of 7 kHz. After a second prism compressor stage, the laser pulses had a width of 100 fs and an energy of approximately 15 μJ. The laser beam was then split by a dielectric beamsplitter into a pump beam ($\mathbf{k}_e$) passing through an optical delay line and into a probe beam ($\mathbf{k}_p$), as shown in Fig. 1.

Crystal polarizers in the two beams were adjusted for vertical, i.e., *s* polarization. Both beams were focused with a 175-mm lens onto the sample to spot sizes of roughly 400 μm diam. The angle θ between the two incident beams was 3°. The sample, a 10-μm-thick Si(100) single crystal was glued onto a 1-cm-thick quartz-cube substrate, which was mounted in a computer-driven rotation stage in order to change the angular orientation of the crystal with respect to the polarization direction of the incident laser pulses. The transmission of the silicon sample was measured in a cw spectrometer to be 5% at $\lambda = 620$ nm. The diffracted DFWM signal emitted in the direction $2\mathbf{k}_p - \mathbf{k}_e$ (i.e., under an angle $-\theta$ with respect to the probe beam) was detected with a photomultiplier tube (1P28) positioned after an analyzer controlling the polarization of the diffracted light. We used two lock-in amplifiers in series driven at the two different reference frequencies of the pump-and-probe beam, which were chopped with 180 Hz and 3.3 kHz, respectively, to get a background-free signal. A $\lambda/2$ plate for 620 nm was used to adjust the laser polarization in either the pump or the probe beam.

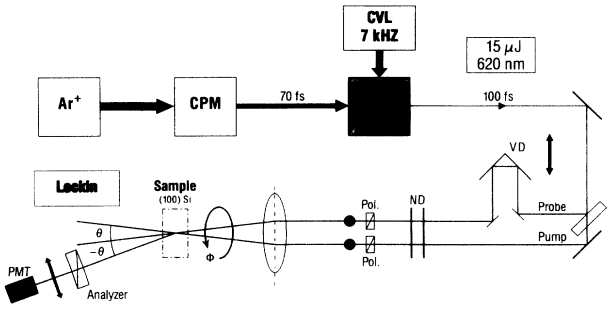

FIG. 1. Experimental setup. For details, see the text.

III. THEORY

Theoretical expressions for the third-order nonlinear polarization were derived by Armstrong *et al.*,[21] and the waves created by this polarization, both in reflection and transmission, were discussed in detail by Bloembergen and Pershan.[22] The comprehensive study of third-order nonlinear processes was carried out by Maker and Terhune.[23] Sipe, Moss, and van Driel presented a phenomenological theory for anisotropic second- and third-harmonic generation obtained in reflection from the surface and the bulk of cubic centrosymmetric single crystals.[9] The theory of DFWM is entirely analogous and the purpose of this section is merely to present the equations necessary to derive the nonlinear susceptibility $\vec{\chi}^{(3)}$ from the experimental observations.

In nonlinear materials, the induced third-order polarization responsible for the emission of light in the $2\mathbf{k}_p - \mathbf{k}_e$ direction (see Fig. 3) can be written as

$$\mathbf{P}^{(3)}(\omega) = \vec{\chi}^{(3)}(\omega;\omega,\omega,-\omega) \vdots \mathbf{E}^{(p)}(\omega)\mathbf{E}^{(p)}(\omega)\mathbf{E}^{(e)}(\omega) , \quad (1)$$

where the fields $\mathbf{E}^{(e)}$ and $\mathbf{E}^{(p)}$ on the right-hand side are the excitation and probe fields inside the medium, respectively. The high rank of the nonlinear susceptibility tensor, fourth rank for $\vec{\chi}^{(3)}$, gives rise to anisotropic DFWM in cubic crystals, in which the intensity of the diffracted beam varies with the relative polarization orientation of the interacting beams. For example, a Si (100) face when illuminated with two *s*-polarized light beams will yield a *p*-polarized diffracted beam whose intensity varies as $\sin^2(4\phi)$, where ϕ is the azimuthal angle of the surface, thereby displaying the fourfold symmetry of Si (100), as indicated in Fig. 2.

For cubic media, the polarization-density-source term responsible for the $-\Theta$ direction diffracted beam can be written as[9]

$$P_i^{(3)} = \chi_{1212}^{(3)}[2(\mathbf{E}^{(e)}\mathbf{E}^{(p)})E_i^{(p)} + (\mathbf{E}^{(p)}\mathbf{E}^{(p)})E_i^{(e)}] + (\chi_{1111}^{(3)} - 3\chi_{1212}^{(3)})(E_i^{(e)}E_i^{(p)}E_i^{(p)}) . \quad (2)$$

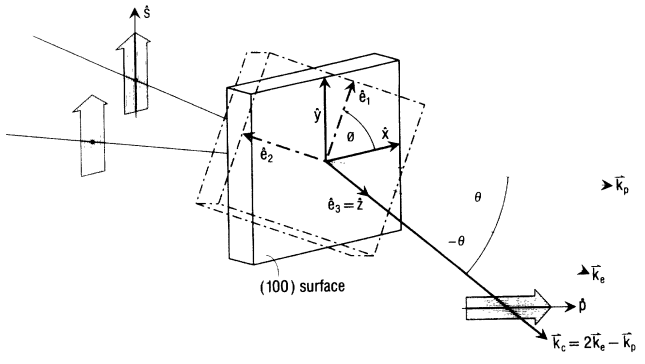

FIG. 2. Schematic of the propagation and polarization configurations considered in the text.

The first term on the right generates a DFWM response, which is isotropic and therefore independent of ϕ; the second term on the right side leads to anisotropic behavior. In order to calculate the DFWM response as a function of ϕ, it is necessary to transform the anisotropic term to the laboratory frame. The anisotropic term can be simplified using the complex cubic anisotropy parameter σ,

$$\chi^{(3)}_{1111}-3\chi^{(3)}_{1212}=-\sigma\chi^{(3)}_{1111} . \tag{3}$$

To describe the rotation of the sample by ϕ about its surface normal, one must transform $\chi^{(3)}_{1111}=\chi^{(3)}_{2222}=\chi^{(3)}_{3333}$ from the cubic crystal axis, $\hat{\mathbf{e}}_1$, $\hat{\mathbf{e}}_2$, and $\hat{\mathbf{e}}_3$, to the laboratory coordinate system, $\hat{\mathbf{x}}$, $\hat{\mathbf{y}}$, and $\hat{\mathbf{z}}$. As shown in Fig. 2, the unit vectors $\hat{\mathbf{e}}_3$ and $\hat{\mathbf{z}}$ are defined as normal to the plane of incidence. The azimuthal angle ϕ is defined such that for $\phi=0°$, $\hat{\mathbf{e}}_1$ and $\hat{\mathbf{e}}_2$ are parallel to $\hat{\mathbf{x}}$ and $\hat{\mathbf{y}}$, respectively. For a rotation of the sample by ϕ about $\hat{\mathbf{z}}$, $\chi^{(3)}_{pqrs}$ transforms according to

$$[\chi^{(3)}_{ijkl}]'=R_{ip}(\phi)R_{jq}(\phi)R_{kr}(\phi)R_{ls}(\phi)\chi^{(3)}_{pqrs} , \tag{4}$$

where $\{R_{ij}(\phi)\}$ is the matrix for the transformation between the cubic crystal coordinate system and the laboratory coordinate system. $\{R_{ij}(\phi)\}$ takes the form

$$\{R_{ij}(\phi)\}=\begin{bmatrix}\cos\phi & -\sin\phi & 0\\ \sin\phi & \cos\phi & 0\\ 0 & 0 & 1\end{bmatrix} . \tag{5}$$

The anisotropic $[\chi^{(3)}_{ijkl}]$ components, given with respect to the laboratory coordinate system, are listed in Table I. We will discuss two geometries for the excitation and probe experiment: parallel and orthogonal geometries in which the electric polarization of the diffracted field $\mathbf{E}^{(c)}$ is either parallel or orthogonal to the y direction. In both geometries, the polarization of the excitation field $\mathbf{E}^{(e)}$ and probe field $\mathbf{E}^{(p)}$ is parallel to the y direction. Note that our definition of the orthogonal configuration differs from the one given by Wherrett, Smirl, and Boggess[24] in that here $\mathbf{E}^{(c)}$ is perpendicular to $\mathbf{E}^{(p)}$ allowing investigation of a purely anisotropic DFWM signal. The excitation and probe beams are taken to propagate in the x-z plane (Fig. 2) with wave vectors $\mathbf{k}_e$ and $\mathbf{k}_p$, respectively. The diffracted beam propagates with a wave vector of $\mathbf{k}_c=2\mathbf{k}_p-\mathbf{k}_e$. It should be noted that the two-pulse self-diffraction geometry in principle implies a small phase mismatch $\Delta\mathbf{k}$, where $\Delta k=|2\mathbf{k}_p-\mathbf{k}_e-\mathbf{k}_c|$ is the wave-vector mismatch between the generated signal wave and the driving polarization field. To determine the DFWM intensity $I_c(\phi)$ as a function of ϕ, recall that the excitation and probe fields in Eq. (2) are inside the crystal, whereas $I_c(\phi)$ is measured outside the crystal. Therefore, the tensor elements in the beam frame, $\chi^{(3)}_{ijkl}$, have to be multiplied by the appropriate Fresnel factors. In all our experiments, the interacting beams propagate within less than 3° with respect to the surface normal; therefore, we can neglect the z component of the electrical fields $\mathbf{E}^{(e)}$, $\mathbf{E}^{(p)}$, and $\mathbf{E}^{(c)}$. This approximation is reasonable, since the only $\chi^{(3)}_{ijkl}$ component involving a z component of the electrical fields is $\chi^{(3)}_{zzzz}$ (see Table I), which scales with $\sin^4\theta\approx10^{-7}$. We can now express $\mathbf{E}^{(c)}$ in terms of the isotropic component $B=3\chi^{(3)}_{1221}$ and the anisotropic component $A-B=\chi^{(3)}_{1111}-3\chi^{(3)}_{1221}$ as a function of ϕ for the parallel configuration [see Table I and Eq. (2)]

$$E^{(c)}_y(\phi)=\{B+\tfrac{1}{4}[3+\cos(4\phi)](A-B)\}E^{(e)}_yE^{(p)}_yE^{(p)}_y , \tag{6a}$$

and for the orthogonal geometry

$$E^{(c)}_x(\phi)=\tfrac{1}{4}[\sin(4\phi)(A-B)]E^{(e)}_yE^{(p)}_yE^{(p)}_y . \tag{6b}$$

Finally, joining Eqs. (6a) and (6b) results in the following expression for the intensity of the diffracted beam with arbitrary linear polarization:

$$\begin{aligned} I_c(\phi,\alpha)&\propto|E^{(c)}_x(\phi)\cos\alpha+E^{(c)}_y(\phi)\sin\alpha|^2\\ &\propto|\tfrac{1}{4}(A-B)\{[3+\cos(4\phi)]\sin\alpha+\sin(4\phi)\cos\alpha\}\\ &\quad+B\sin\alpha|^2 , \end{aligned} \tag{7}$$

where α represents the angle between the x axis and $\mathbf{E}^{(c)}$.

IV. RESULTS AND DISCUSSION

To investigate the presence of the anisotropic component $(A-B)$, we first consider the intensity of the diffracted beam $I_c(\phi,\alpha)$ at zero time delay between the excitation and probe pulse as a function of ϕ. Figure 3(a) shows the experimental measurements of $I_c(\phi,\alpha)$ obtained by setting $\alpha=0°$. The fourfold symmetry of $E^{(c)}_x$ [see Eq. (6b)] leads to an eightfold intensity pattern as a function of ϕ. The solid line in Fig. 3(a) is a fit of Eq. (7) to the experimental data. As stated above, the results of Fig. 3(a) were achieved by setting the polarization of the diffracted beam perpendicular to the polarization of the

TABLE I. Anisotropic $[\chi^{(3)}_{ijkl}]$ components of the (100) surface. The prefactor $-\sigma\chi^{(3)}_{1111}$ and zero $[\chi^{(3)}_{ijkl}]$ components have been omitted.

i \ jkl	xxx	yyy	zzz	xxy	yyx
x	$\frac{1}{4}[3+\cos(4\phi)]$	$-\frac{1}{4}\sin(4\phi)$	0	$\frac{1}{4}\sin(4\phi)$	$\frac{1}{4}[1-\cos(4\phi)]$
y	$\frac{1}{4}\sin(4\phi)$	$\frac{1}{4}[3+\cos(4\phi)]$	0	$\frac{1}{4}[1-\cos(4\phi)]$	$-\frac{1}{4}\sin(4\phi)$
z	0	0	1	0	0

excitation and probe beam. Obviously, it is essential to check the perpendicular adjustment of the polarizations and to consider the accuracy to which the polarizations of the incident beams can be defined. It is possible to set the excitation and probe polarization directions parallel within an accuracy given by the extinction ratio of the polarizers ($\sim 10^{-5}$). Therefore, the observed isotropic contribution in $I_c(\phi,\alpha)$ [see Fig. 3(a)] can be attributed to arise from a leakage of the parallel component of the diffracted beam $E_y^{(c)}(\phi)$ through the imperfectly crossed analyzer ($\alpha \cong 0°$).

This is not surprising, as the light must pass through a quartz lens, the sample, and the substrate before encountering the analyzer. We can measure this signal by rotating the analyzer so that it passes a small contribution of x-polarized light. The results of this measurement are shown in Figs. 3(b) and 3(c) where the analyzer was rotated $+3°$ and $-3°$ away from the x direction. Figure 3(b) shows that the isotropic amplitude B and the anisotropic term $(A-B)$ must be of the same order of magnitude when the analyzer is rotated 3° away from the x direction. However, rotating the analyzer by $-3°$ away from the x direction results in a sign change of the isotropic term B, due to a change of the sign of $\sin\alpha$. This behavior is manifested in the differences between the rotation patterns of $I_c(\phi,+3°)$ and $I_c(\phi,-3°)$, as shown in Figs. 3(b) and 3(c), respectively.

In order to demonstrate the sensitivity of $I_c(\phi,\alpha)$ on α, we have calculated $I_c(\phi,\alpha)$ as a function of α for different azimuthal angles, $\phi=0°$, 22.5°, 45°, and 67.5°; the results are plotted in Fig. 4 corresponding to curves (a)–(d), respectively, and we used a value of $|\sigma| \cong 0.21$ in our calculation as determined from Figs. 3(b) and 3(c). Curves (a) and (c) in Fig. 4 indicate that the minima in Fig. 3(a) should vanish for exactly crossed ideal polarizers, $\alpha=0°$, but should increase parabolically with $|\alpha|$, as given in Eq. (7). The sensitivity of $I_c(\phi,\alpha)$ on the polarization angle α is manifested in the disappearance of curves (b) and (d) at $\alpha \cong -3°$ and $+3°$, respectively. This means that the first and second maxima in Fig. 3(a) become minima, as one can infer from Figs. 3(b) and 3(c).

Similar variations of the diffracted signal intensity in dependence on the rotation angle ϕ are observed if instead of the analyzer in the signal beam the polarization of the pump beam is turned by a small angle α. This behavior can be derived from the symmetry given in Table I.

However, the DFWM signal is insensitive to the polarization direction of the probe beam as no isotropic contribution to $\mathbf{E}^{(c)}$ is allowed[9] under crossed polarization of probe and diffracted beams, as long as the pump beam is linearly polarized. Figure 5 presents the theoretically predicted variation of the signal intensity $I_c(\phi=22.5°,\alpha)$ as a function of α if either the polarization of the signal, pump, or probe beam is slightly tilted.

In fact, the high sensitivity of the rotation pattern to small admixtures of an isotropic contribution to the purely anisotropic component expected for exactly perpendicular orientation of the analyzer in the signal path to both

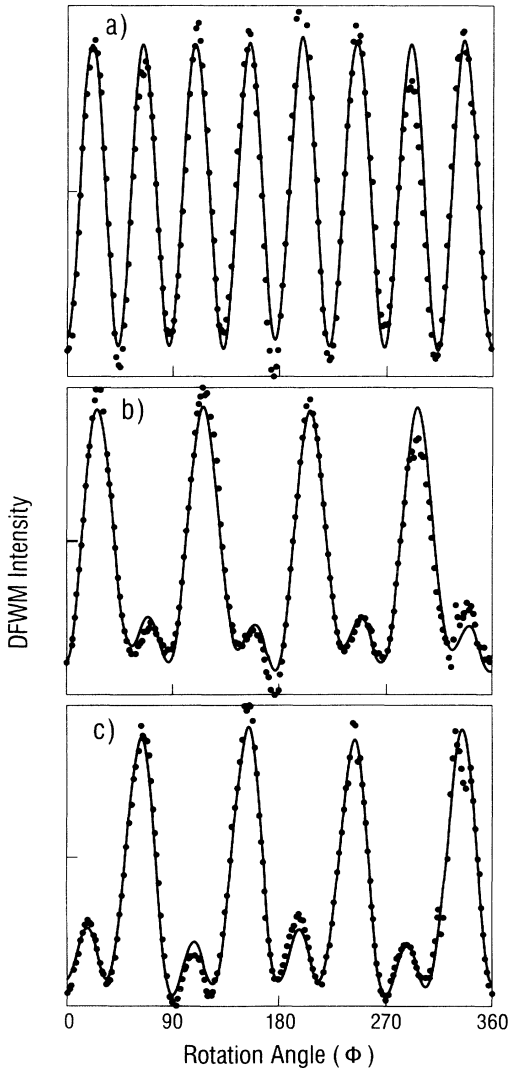

FIG. 3. DFWM signal (●) vs azimuthal angle ϕ for (a) $\alpha=0°$, (b) $\alpha=+3°$, and (c) $\alpha=-3°$ deviation of the signal polarization direction from p polarization. In each case the pump-and-probe beams were s polarized. The solid lines are fits using Eq. (7).

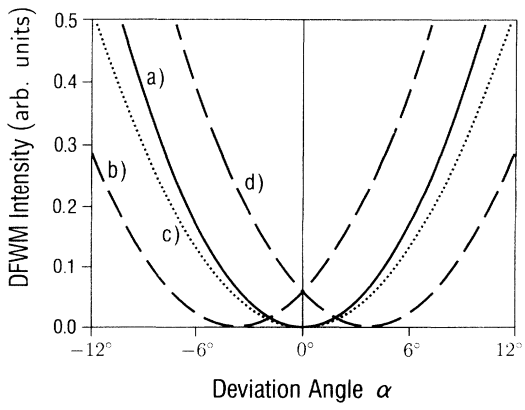

FIG. 4. DFWM signal calculated as a function of the deviation α from p polarization for different azimuthal orientations of the Si sample: curve (a) $\phi=0°$, (b) $\phi=22.5°$, (c) $\phi=45°$, and (d) $\phi=67.5°$.

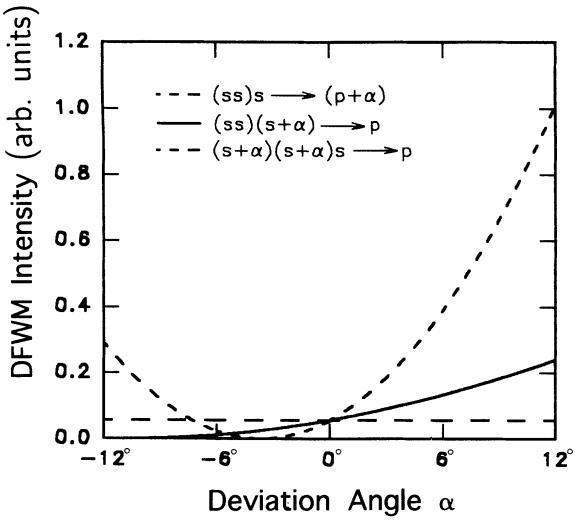

FIG. 5. DFWM signal $I_c(\phi=22.5°)$ vs α for deviating polarization of the signal (solid line), the pump (dotted line), or the probe beam (dashed line).

the pump-and-probe-beam polarization allows monitoring of the photoexcited carrier dynamics on a very short time scale.

For this purpose, a variable delay τ was introduced into the path of the probe beam (as shown in Fig. 1), such that for positive delays the excitation pulse precedes the probe pulse into the sample. Figure 6 presents a plot of the time-integrated intensity diffracted into the direction $2\mathbf{k}_p - \mathbf{k}_e$ versus the time delay between the two pulses. The temporal width of the signal (130 fs) more or less resembles that of the profile corresponding to third-order convolution of the laser pulses. This observation proves that phase memory effects of the coherent polarization created by the first pulse must be extremely short lived and are hard to detect as an asymmetry of the signal shape. The anisotropic signal can be attributed to the achievement of anisotropic state filling in silicon, whereas the isotropic amplitude B is associated with isotropic excitation of states in k space.

Recall that the population created by the first pulse, which is expected to be long lived compared to the pulse time, is not observable in a two-pulse self-diffraction experiment if the time delay is large compared to the optical dephasing time since generation of a signal diffracted into the direction $2\mathbf{k}_p - \mathbf{k}_e$ necessitates coherent interaction between the field of the second pulse and the coherent polarization left behind by the first pulse. Therefore, the isotropic amplitude is expected to decay with the dephasing time.

The anisotropic term $(A - B)$, associated with anisotropic state filling, decays preferentially by momentum relaxation but the optical coherence becomes completely negligible only after energy relaxation. In silicon, the intravalence-band energy relaxation time T_v is about 1 ps,[25] whereas the reorientational diffusion time T_0 has been found to be much shorter than 1 ps.[26] Hence, while the direct effect of the radiation is to create excited carriers with a preferential momentum orientation in k space (anisotropic state filling), momentum randomization and intraband-energy relaxation will lead to a rapid decay of the anisotropy. For excitation densities of $\geq 10^{18}$ cm^{-3}, as used in the present experiments, phase relaxation due to electron-electron, hole-hole, and electron-hole scattering is expected to occur on a time scale of 10 fs.

The anisotropic contribution to the DFWM signal, which is measured by the crossed polarization configuration utilized in our experiment exhibits a significant time delay by approximately 20 fs with respect to the total diffracted intensity, which has been monitored independently by a second detector and is depicted as the dashed trace in Fig. 6. This result becomes explainable if one assumes an additional isotropic contribu-

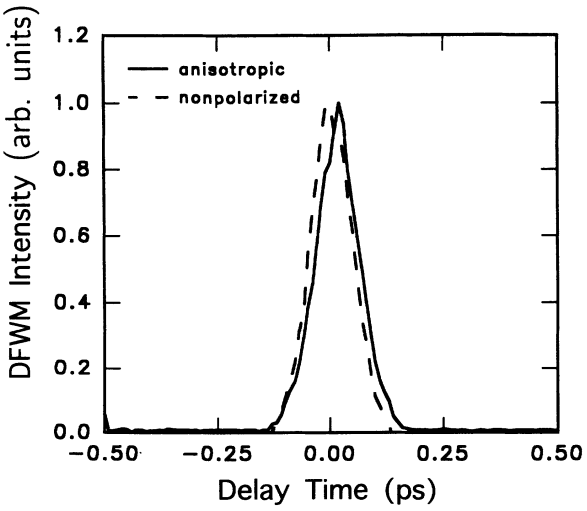

FIG. 6. Anisotropic (solid line) and total (dashed line) DFWM signal measured as a function of the delay τ between the two pulses.

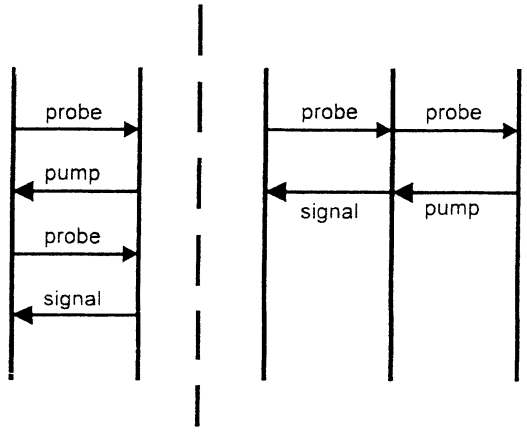

FIG. 7. Pulse-mixing schemes for negative (top) and positive (bottom) delay τ between the pump and probe pulses.

tion for negative delays when pulse two contributing two photons to the DFWM signal arrives before pulse one. For this pulse sequence, the mixing occurs via the scheme depicted in the top part of Fig. 7, whereas for positive delays, it is dominated by the third-order polarization of the interband transition shown in the bottom part of Fig. 7. From this result we have to conclude that the polarization path involving transitions between the lowest and higher conduction bands has a lower anisotropy than the valence lowest conduction-band transition.

We have performed measurements of $I_c(\phi,\alpha\approx 0°)$ as a function of ϕ for different delay times τ. The results are shown in Figs. 8(a) and 8(b) for delays of -70 fs (dashed line) and $+70$ fs (solid line), and 0 fs (solid line) and $+25$ fs (dashed line). As can be seen from Fig. 8, the variation of I versus ϕ changes tremendously with the delay time between the excitation and probe pulses. Comparison of Fig. 8 with Fig. 3 suggests that the time delay leads to the increased influence of the isotropic component on the measured signal pattern similar to slight rotations of the polarizers for the pump or the signal beam. The increasing importance of the isotropic as compared to the anisotropic part of the signal with increasing delay points to slightly different relaxation times of the isotropic and anisotropic contribution to the polarization created by the first pulse. This observation confirms that momentum randomization is faster than intraband-energy relaxation but does not result in a complete loss of the phase coherence.

The traces recorded for negative and positive time delay τ reveal the same differences as the curves measured for positive and negative α. According to Eq. (7), we thus have to conclude that the sign of the isotropic component must be opposite for positive and negative delays. In particular this result excludes imperfect perpendicular orientation of the polarizer in the signal beam with respect to the polarization of the two exciting beams since a small isotropic component originating from slight misorientation of the polarizers should have the same sign independent of the delay.

The experimental finding is understandable if the additional isotropic contribution created by the pulse-mixing sequence $\mathbf{k}_p+\mathbf{k}_p-\mathbf{k}_e$ for $\tau\leq 0$ has the opposite sign and is larger than the isotropic signal due to the sequence $-\mathbf{k}_e+\mathbf{k}_p+\mathbf{k}_p$.

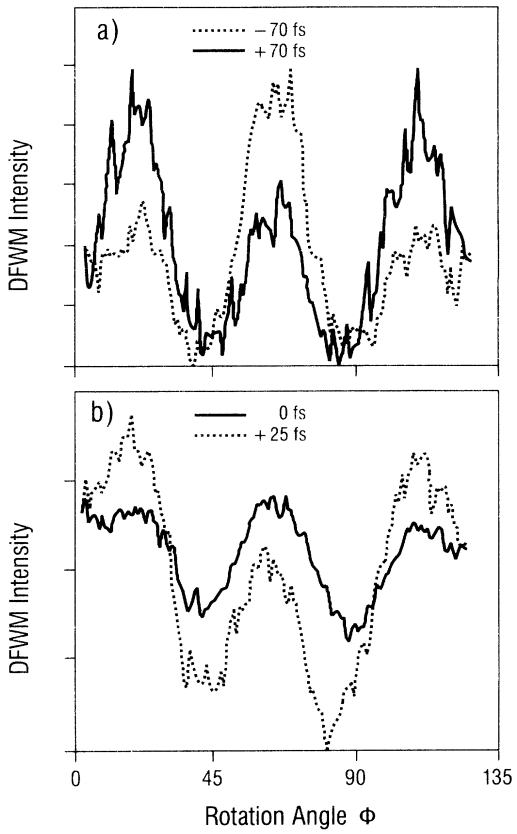

FIG. 8. DFWM signal vs azimuthal angle ϕ for different time delays between the pump-and-probe pulses: (a) -70 fs (dashed line), $+70$ fs (solid line) and (b) $+25$ fs (dashed line), 0 fs (solid line).

V. SUMMARY

We have presented experimental and theoretical results for the cubic anisotropy of the third-order susceptibility for femtosecond DFWM in crystalline silicon. A detailed study of the rotation patterns exhibiting the fourfold symmetry of the [100] direction has been performed with respect to the polarization of the pump, probe, and the diffracted beam. The sensitivity of the anisotropy to delay times between the pump and probe beam of less than 10 fs suggests that DFWM can be a useful probe of not only the symmetry of the potential in which the electrons move but also of the details of that motion.

Preliminary time-resolved measurements indicate that the isotropic component of $\vec{\chi}^{(3)}$ is dominated by band-filling processes, while the anisotropic component exhibits the behavior of anisotropic state filling in k space.

[1]See, for example, special issue IEEE J. Quantum Electron. **QE-22** (1986).

[2]D. S. Chemla, D. A. B. Miller, P. W. Smith, A. C. Gossard, and W. Wiegmann, IEEE J. Quantum Electron. **QE-22**, 265 (1984).

[3]C. Weber, U. Becker, R. Renner, and C. Klingshirn, Appl. Phys. B **45**, 113 (1988).

[4]H. J. Eichler, P. Günter, and D. W. Pohl, *Laser Induced Dynamic Gratings* (Springer-Verlag, Berlin, 1986).

[5]H. J. Eichler, F. Massmann, E. Biselli, K. Richter, M. Glotz, L. Konetzke, and X. Yang, Phys. Rev. B **36**, 3247 (1987), and references therein.

[6]A. L. Smirl, T. F. Boggess, B. S. Wherrett, G. P. Perryman, and A. Miller, IEEE J. Quantum Electron. **QE-19**, 690 (1983).

[7]V. M. Petnikova, S. A. Pleshano, and V. V. Shuvalov, Sov. JEJ

88, 360 (1985).
[8]M. A. Vasil'Eva, J. Vischakas, V. Kabelka, and A. V. Masalov, Opt. Commun. **53**, 412 (1985).
[9]J. E. Sipe, D. J. Moss, and H. M. van Driel, Phys. Rev. B **35**, 1129 (1987).
[10]D. J. Moss, H. M. van Driel, and J. E. Sipe, Appl. Phys. Lett. **48**, 1150 (1986).
[11]C. C. Wang, J. Bomback, W. T. Donlon, C. R. Huo, and J. V. James, Phys. Rev. Lett. **57**, 1647 (1986).
[12]E. C. Fox and H. M. van Driel, IEEE J. Quantum Electron. **QE-25**, 1104 (1989).
[13]C. C. Wang and N. W. Ressler, Phys. Rev. B **2**, 1827 (1979).
[14]J. J. Wynne, Phys. Rev. **178**, 1295 (1969).
[15]E. Yablonovitch, C. Flytzanis, and N. Bloembergen, Phys. Rev. Lett. **29**, 865 (1972).
[16]W. K. Burns and N. Bloembergen, Phys. Rev. B **4**, 3437 (1971).
[17]D. J. Moss, H. M. van Driel, and J. E. Sipe, Opt. Lett. **14**, 57 (1989).
[18]R. L. Fork, B. I. Greene, and C. V. Shank, Appl. Phys. Lett. **38**, 671 (1981); R. L. Fork *et al.*, IEEE J. Quantum Electron. **QE-19**, 500 (1983).
[19]R. L. Fork *et al.*, Opt. Lett. **9**, 150 (1984).
[20]W. H. Knox *et al.*, Opt. Lett. **9**, 552 (1984).
[21]J. A. Armstrong, N. Bloembergen, J Ducuing, and P. S. Pershan, Phys. Rev. **127**, 1918 (1962).
[22]N. Bloembergen and P. S. Pershan, Phys. Rev. **128**, 606 (1962).
[23]P. D. Maker and R. W. Terhune, Phys. Rev. **137**, 801 (1965).
[24]B. S. Wherrett, A. L. Smirl, and T. F. Boggess, IEEE J. Quantum Electron. **QE-19**, 680 (1983).
[25]J. A. Lietoila and J. F. Gibbons, Appl. Phys. Lett. **40**, 624 (1982).
[26]H. Bergner, V. Brückner, and M. Supianek, IEEE J. Quantum Electron. **QE-22**, 1306 (1986).

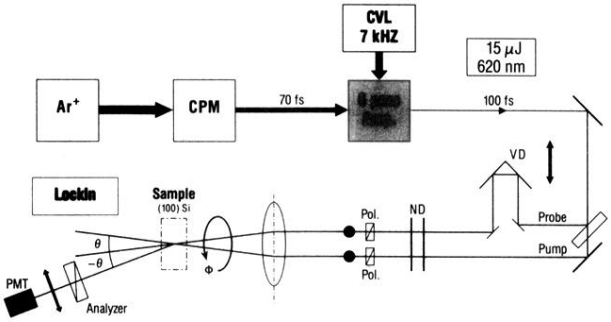

FIG. 1. Experimental setup. For details, see the text.

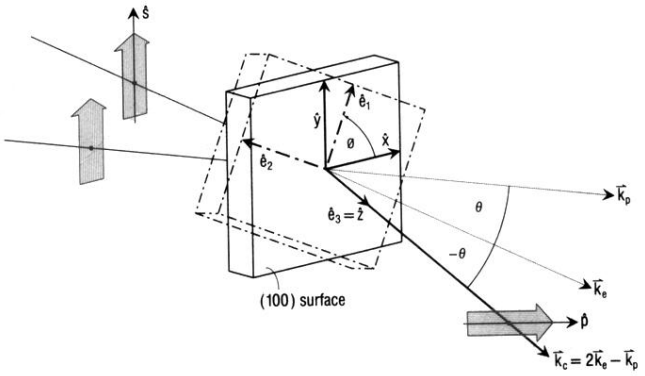

FIG. 2. Schematic of the propagation and polarization configurations considered in the text.